

DESY 96-101

June 1996

Higgs and Top Production in the Reaction $\gamma e \longrightarrow \nu b \bar{b} W$ at TeV Linear Collider Energies

E. Boos¹, A. Pukhov¹, M. Sachwitz² and H. J. Schreiber²

¹Institute of Nuclear Physics, Moscow State University, 119899, Moscow,
Russia

²DESY-Institut für Hochenergiephysik, Zeuthen, FRG

arXiv:hep-ph/9610424v1 20 Oct 1996

Abstract

For an electron-photon collider the complete tree-level cross sections of the reaction $\gamma e \rightarrow \nu b \bar{b} W$ are computed at center-of-mass energies between 0.5 and 2.0 TeV, for top masses of 160 to 200 GeV and Higgs masses between 80 and 140 GeV within the Standard Model. It is shown that most of the $\nu b \bar{b} W$ events are due to Higgs and Z/γ^* production (with $H, Z/\gamma^* \rightarrow b \bar{b}$ decay) while top production (with $t \rightarrow b W$ decay) is about 50% smaller. Multiperipheral background and interferences are small, respectively negligible, in the energy range studied. By convoluting the basic cross sections with an energy spectrum of the backscattered photon beam, and inserting linear collider luminosities as anticipated in present designs, realistic $\nu b \bar{b} W$ event rates are estimated. This results in large event rates for $\gamma e \rightarrow \nu t b$ and $\gamma e \rightarrow \nu H W$. We estimate that the CKM matrix element $|V_{tb}|$ can be probed from the $\nu t b$ final state to an accuracy of 1-3% at $\sqrt{s_{e^+e^-}} \gtrsim 1$ TeV. Assuming an effective Lagrangian based on dimension-6 operators we discuss the sensitivity for detecting deviations of the $H W W$ coupling from the Standard Model in the reaction $\gamma e \rightarrow \nu H W$.

1 Introduction

Electron-photon and photon-photon colliders are seriously considered as interesting options to upgrade future linear e^+e^- colliders. The electron-photon and photon-photon collisions have been to a great extent studied in the context of e^+e^- physics by using virtual bremsstrahlung and beamstrahlung photons. However, γe and $\gamma\gamma$ colliders where the photon beams are generated by backward Compton scattering of laser light on the high energy electron beams supplied by the underlying e^+e^- collider, have great advantages. The mechanism of the electron to photon beam conversion has been studied theoretically by many authors, see e.g. [1, 2]. According to their results, the typical photon beam energy is about 0.7 times the electron beam energy. Thus, the γe collision energy is roughly 80% of the underlying e^+e^- collider energy. If the polarizations of the source electron beam and the laser photon can be controlled, the resulting photon beam can be almost monochromatic and highly polarized.

With increasing collision energy the complexity of the events is expected to increase. While at the Z^0 peak (LEP-1 energy) two-fermion final states produced by the Z^0 decay are, by far, the most important processes, 4-fermion final states become dominant at LEP-2 due to W^+W^- production. It is expected that at higher energies many-body reactions with fermions and vector bosons in the final state will play a growing part. Such reactions may yield additional or complementary, or even more stringent, information about couplings of e.g. the Standard Model (SM) [3] Higgs boson and the top quark, or may reveal deviations from SM predictions in more obvious ways.

In this paper we analyze the reaction

$$\gamma e \rightarrow \nu b \bar{b} W^- \quad (1)$$

at high center of mass (cm) energies. We do not focus on low energy γe reactions from Weizsäcker-Williams [4] and beamstrahlung photons which will be automatically generated in e^+e^- collisions. We assume that the backscattered photon beam is unpolarized and that, on the average, the number of the backscattered photons produced per positron is close to 1. Interactions of quarks (and gluons), created by perturbative $q\bar{q}$ (gluons) fluctuations of the real photon, are not taken into account in the present paper.

Reaction (1) is interesting on its own because it simultaneously involves single top quark production in the subreaction

$$\gamma e \longrightarrow \nu \bar{b} t \quad (2)$$

and associated Higgs boson production in

$$\gamma e \longrightarrow \nu W^- H^0, \quad (3)$$

with subsequent decays of the top, $t \longrightarrow Wb$, and respectively, the Higgs, $H \longrightarrow b\bar{b}$. Both reactions have been studied in the past [5, 6] and their abundant rates were emphasized. We note that reaction (2), a subchannel of the process $e^+e^- \longrightarrow evtb$ recently studied by the authors [7], serves as a unique tool to probe the Wtb coupling and to measure the Cabibbo-Kobayashi-Maskawa (CKM) matrix element $|V_{tb}|$ with high precision. Reaction (3) will, due to its large rate, be of special interest for probing the HWW coupling.

In this paper we present results of complete tree-level calculations of the reaction $\gamma e \longrightarrow \nu b\bar{b}W$ within the SM. Decays of unstable particles with correct spin structures and contributions from all nonresonant diagrams are taken into account. In this way, the subreactions (2) and (3) are involved automatically in the 2-to-4 body calculations and, as will be shown, they can easily be extracted from the inherent background leading to the same final state.

The paper is organized as follows. In sect. 2 we introduce the contributing diagrams, the method of calculation, the problem of singularities and the choice of a proper kinematical scheme. Cross sections for reactions (1), (2) and (3) are presented in sect. 3 as function of the photon-electron cm energy $\sqrt{s_{\gamma e}}$. Higgs and top masses are varied between 80 and 140 GeV and 160 and 200 GeV, respectively. In sect. 4 the cross sections of reactions (1)-(3) are folded with an assumed energy spectrum of the backscattered photon beam. In this way, the impact of the model-dependent photon spectrum of ref. [1] on the expected event rate is illustrated. Sect. 5 is devoted to the prospects of measuring the matrix element $|V_{tb}|$, while in sect. 6 the detection of possible anomalous Higgs couplings to W^+W^- bosons is discussed. Sect. 7 contains the summary.

2 Diagrams, singularities and kinematical scheme

All SM tree-level diagrams contributing to the reaction $\gamma e \rightarrow \nu b \bar{b} W$ are shown in Fig. 1. Only contributions from the physical particles are presented. Diagrams for Faddeev-Popov's ghosts and Goldstone bosons are omitted. Their contributions were however taken into account in the t'Hooft-Feynman gauge.

The three diagrams in the first row of Fig. 1 involve the Higgs boson production with its decay to $b \bar{b}$. Top production (with subsequent $t \rightarrow b W$ decay) occurs in diagrams (4)-(7) in the second row. Both these classes of diagrams are denoted '*signal diagrams*' in the following. In diagrams (8)-(16) Z and virtual photons are produced with subsequent $Z/\gamma^* \rightarrow b \bar{b}$ decays. The remaining diagrams of Fig. 1 are of multiperipheral nature.

The results presented have been obtained by means of the computer package CompHEP [8]. The present version of CompHEP performs analytic calculations of the matrix elements squared, generates an optimized Fortran code and generates a flow of events. In addition, it provides the possibility for the user to choose an appropriate kinematical scheme.

The basic input parameters used in the program are taken from the report of the Particle Data Group [9] or are as listed here: $m_b = 4.3$ GeV, $\alpha_{EW} = 1/128$, $|V_{tb}| = 0.999$, $M_Z = 91.187$ GeV, $\sin^2 \Theta_W = 0.23$, $M_W = M_Z * \cos \Theta_W$, $\Gamma_Z = 2.50$ GeV and $\Gamma_W = 2.09$ GeV.

For unstable particles, Breit-Wigner formulae have been used for the s-channel propagators. For the Higgs and top the tree-level widths are applied.

As seen from the diagrams in Fig. 1, a number of singularities exists in the s- and t-channels. In the phase space integration by the adaptive Monte Carlo method, a proper treatment of such singular behaviour is necessary in order to obtain stable results. Usually, singularities are smoothed by appropriate transformations of variables, and ref. [10] describes formulae for smoothing of singularities as used in CompHEP, which have been adopted in our calculations.

Smoothing of singularities works effectively only in the case of a proper choice of the kinematical scheme. Basically, we selected integration variables in such a way that each of the singularities occurs in only one of these variables. The choice of the scheme used for reaction (1), $\gamma e \rightarrow \nu b \bar{b} W$, is briefly described in the following, see also Fig. 2:

- in the first step we consider the decay of cluster (12) into particle (3) and cluster (456) in its rest frame. The angle between the three-momenta of particles(2) and (3), Θ_{23} , whose cosine is a linear function of the momentum transfer-squared $t_{23} \equiv t_{e\nu}$, has been chosen as a variable, with a singularity at $t_{23} = M_W^2$;

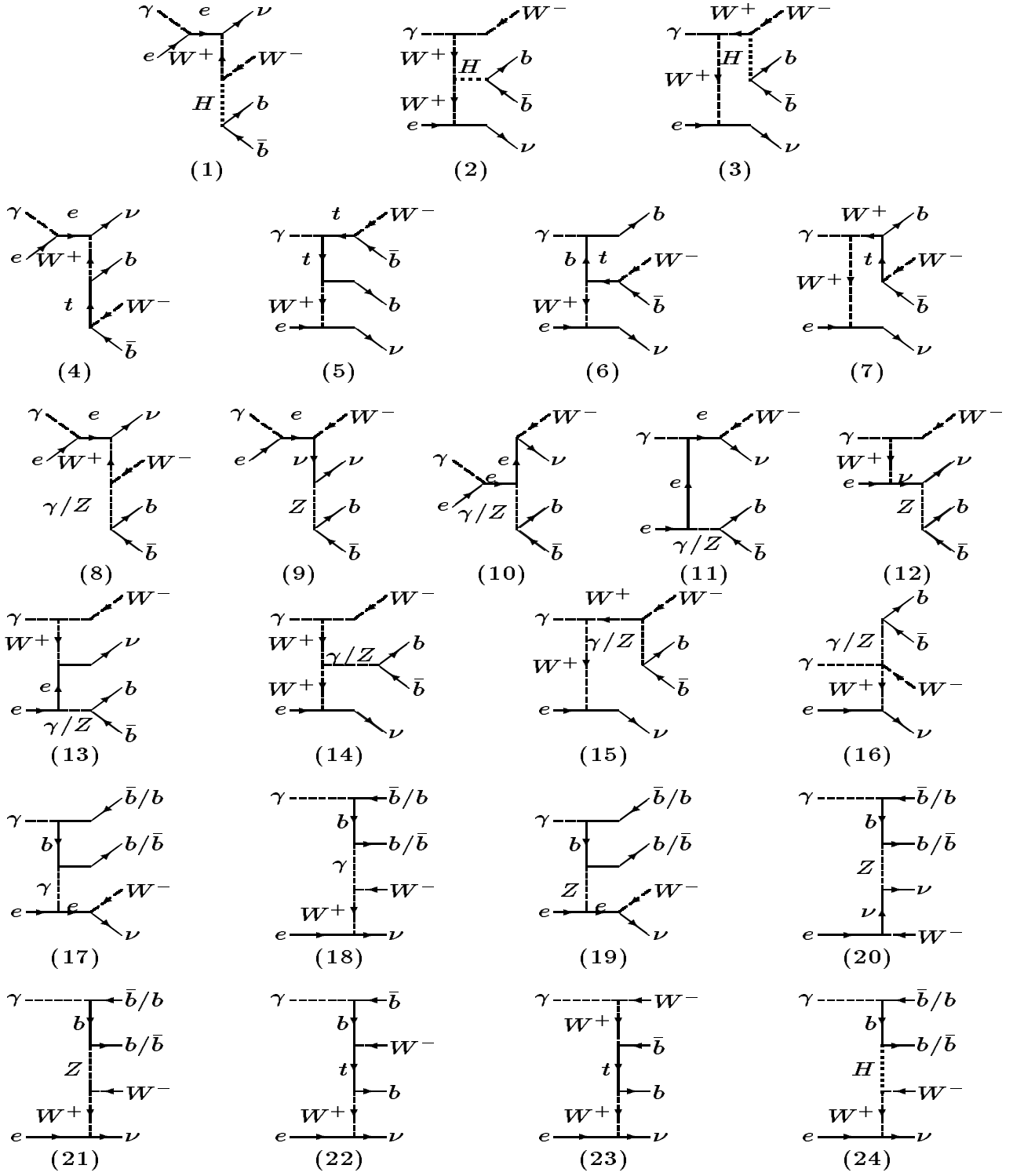


Figure 1: Feynman diagrams for the reaction $\gamma e \rightarrow \nu b \bar{b} W$.

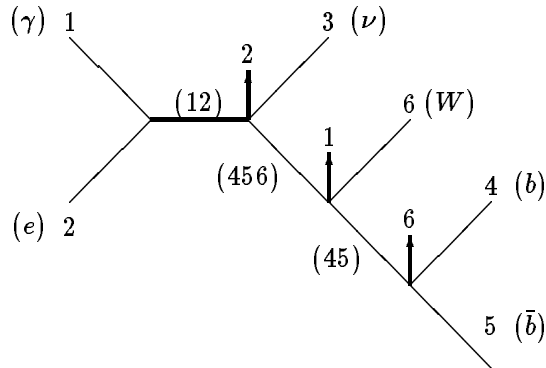


Figure 2: Illustration of the kinematical scheme used in the calculation.

- next, the decay of cluster (456) into particle (6) and cluster (45), considered in its rest frame, offers two angles as variables: Θ_{16} , the angle between particle (1) and (6), and $\Theta_{1(45)}$, that between particle (1) and cluster (45). These angles are linearly related to the momentum transfer-squared $t_{16} \equiv t_{\gamma W}$, and $t_{1(45)} \equiv t_{\gamma(b\bar{b})}$, respectively, having singularities at M_W^2 ;
- selecting the invariant mass of cluster (45), $M_{b\bar{b}}$, as a variable, singularities occur at its threshold and at M_Z and M_H ;
- finally, the decay of cluster (45) into particles (4) and (5) considered in its rest frame, offers the angle Θ_{56} as a variable, which is linearly related to M_{Wb}^2 , with a singularity at m_t^2 .

The singularities mentioned above turned out to be the most important ones and were smoothed according to the description of ref. [10]. In this way we are confident in the stability of our Monte Carlo results.

3 Basic cross section results

In possible future γe colliders, the photon beam will be produced by backscattering of laser light on the high energy electron beam. The photon beam expected from such scatterings will have a nontrivial energy-dependent luminosity spectrum. Its measurement will be crucial so that convolutions with (theoretical) γe reaction cross sections can be performed with high confidence at a given e^+e^- cm energy $\sqrt{s_{e^+e^-}}$. At present, such convolutions must be carried out by means of model-dependent photon spectra. Therefore we present in this paper at first the unconvoluted cross sections for reaction (1) and updated cross sections for reactions (2) and (3), as a function of the γe cm energy $\sqrt{s_{\gamma e}}$. Based on these results the reader can, by using his preferred photon spectrum, carry out convolutions in order to obtain 'realistic' event rate expectations.

Fig. 3 shows the total cross section for reaction (1), $\gamma e \rightarrow \nu b \bar{b} W$, as function of $\sqrt{s_{\gamma e}}$, for a Higgs mass of $M_H = 80$ GeV and a top mass of $m_t = 180$ GeV. It

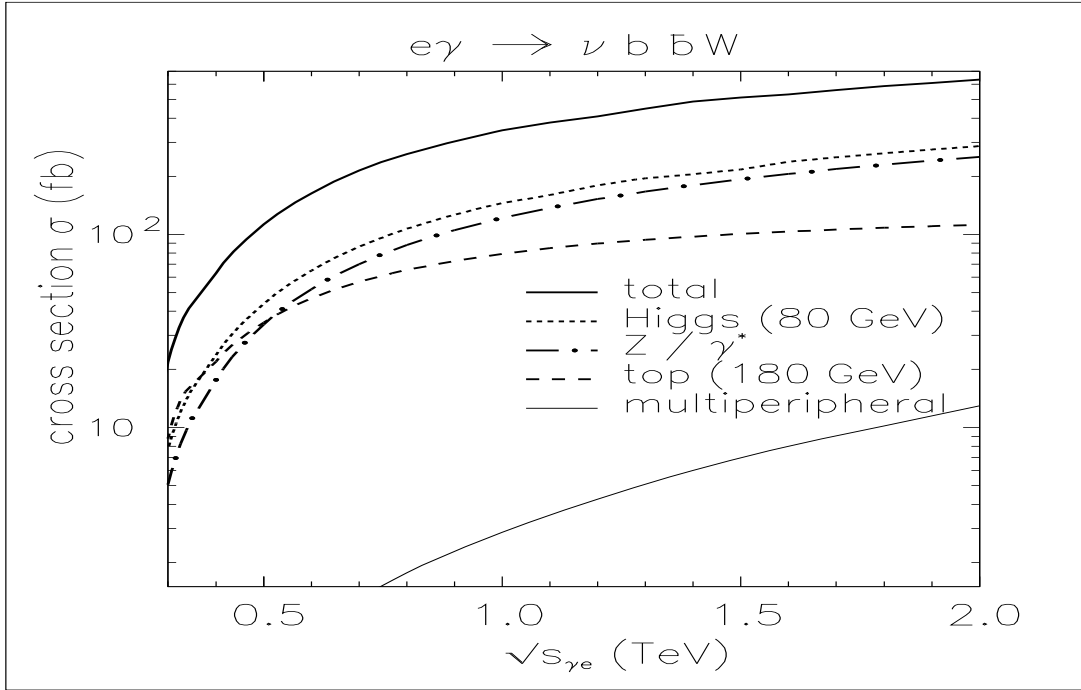


Figure 3: Total cross section for the reaction $\gamma e \rightarrow \nu b \bar{b} W$ as function of the γe cm energy, for $m_t = 180$ GeV and $M_H = 80$ GeV. Also the individual contributions of the Higgs, the top, the Z/γ^* and the multiperipheral diagrams are shown.

rises with increasing energy over the whole energy range considered. Also shown are the cross sections for the single top reaction (2), the Higgs reaction (3), the Z/γ^* and the multiperipheral contributions corresponding to the different classes of diagrams as discussed in sect. 2. The Higgs and the Z/γ^* rates are very close to each other. Top production rises less strongly with increasing energy such that in the 1-2 TeV region, it contributes only about half as much as each of the other two channels. Multiperipheral contributions are, as expected from previous 4-body final state investigations [7], considerably weaker. Still, they are to some extent also responsible for the continuous rise of the overall reaction cross section at high energies.

Table 1 summarizes the cross sections discussed at $\sqrt{s_{\gamma e}} = 0.5, 1.0, 1.5$ and 2.0 TeV.

The total rates given in the first row are accurate to $\lesssim 1.5\%$ by virtue of the choice of an adequate kinematical scheme, despite of non-vanishing masses of the participating particles. All diagrams of Fig. 1 have been included in the calculations. The other numbers in Table 1 obtained from subsets of diagrams have a somewhat better accuracy of $\lesssim 0.2\%$. The interferences between different classes of diagrams shown in the last row rise with increasing energy to significant

Table 1: Cross sections (in fb) for reaction (1) and different subchannels as discussed in the text as well as their interferences.

$\sqrt{s_{\gamma e}}$, TeV	0.5	1.0	1.5	2.0
$\sigma(\text{total})$	113(1)	346(4)	511(5)	634(8)
$\sigma(M_H = 80 \text{ GeV})$	43.7(1)	145.2(2)	224.2(3)	286.3(4)
$\sigma(m_t = 180 \text{ GeV})$	34.9(1)	79.3(1)	100.6(2)	112.2(2)
$\sigma(Z/\gamma^*)$	34.2(1)	121.7(4)	193.0(7)	252.0(9)
$\sigma(\text{Multiperipheral})$.588(2)	2.87(2)	6.91(8)	13.0(2)
Interferences	-1.01(2)	-4.2(1)	-11.7(2)	-23.7(3)

non-zero values at $\sqrt{s_{\gamma e}} = 1.5\text{-}2$ TeV. Their behaviour is similar, apart from the sign, to that of the multiperipheral cross section so that the two contributions cancel each other to some extent. Since interferences between the signal and the Z/γ^* diagrams are consistent with zero, the cross section of reaction (1) is well approximated by their incoherent sum.

The dependence of the cross section for reaction (2) on the top mass m_t and that for reaction (3) on the Higgs mass, M_H , is illustrated in Fig. 4, again as a function of $\sqrt{s_{\gamma e}}$. M_H is varied between 80 and 140 GeV, while m_t is assumed to be 160, 180 and 200 GeV. Away from the thresholds neither a strong Higgs mass nor a strong top mass dependence is observed. The cross sections in each case decrease with increasing mass of the particle in question, as expected from phase space.

It is obvious from Figs.3 and 4 and Table 1 that at large $\sqrt{s_{\gamma e}}$ and moderate Higgs masses (80-140 GeV) the cross sections for reactions (1) - (3) are large so that they become very interesting, from an experimental point of view, for more detailed studies.

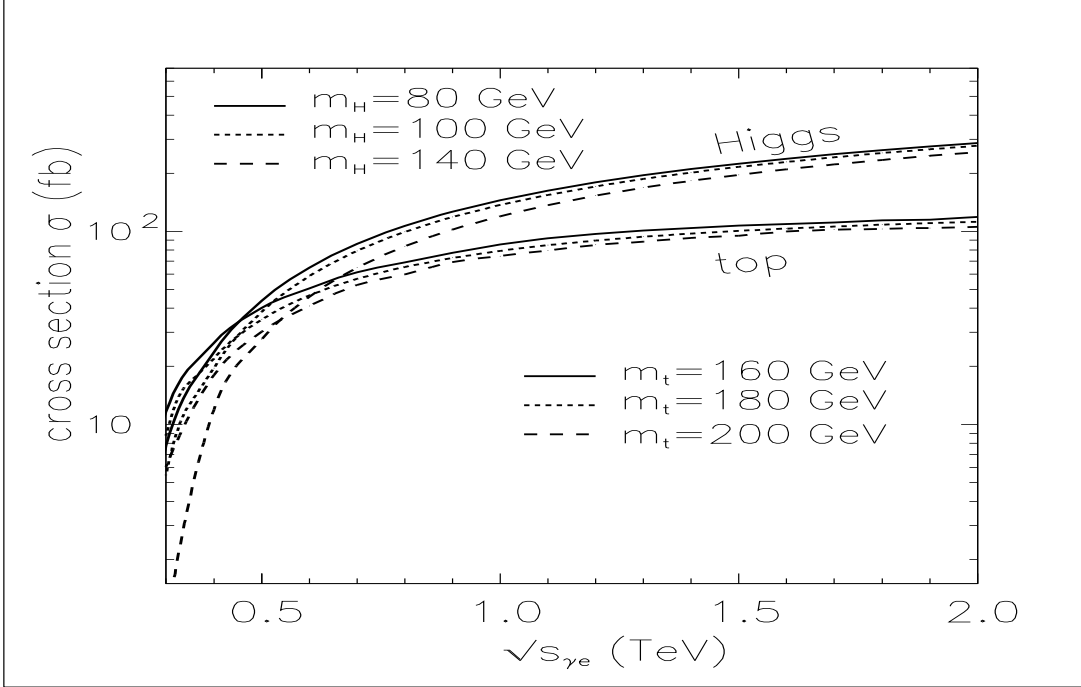


Figure 4: Cross sections for the top and Higgs subreactions as function of the γe cm energy, for $m_{top} = 160, 180$ and 200 GeV and $M_H = 80, 100$ and 140 GeV.

4 Backscattered photon spectrum convoluted cross sections

In order to obtain 'realistic' estimations of event rates expected for reactions (1)-(3) the cross sections of sect. 2 have to be convoluted with the backscattered photon flux. We have, as an example, adopted in our calculations the photon spectrum as proposed in ref. [1]¹

$$F_\gamma = \frac{1}{N(x_0)} \left[1 - y + \frac{1}{1-y} - \frac{4y}{x_0(1-y)} + \frac{4y^2}{x_0^2(1-y)^2} \right]$$

with

$$N(x_0) = \frac{16 + 32x_0 + 18x_0^2 + x_0^3}{2x_0(1+x_0)^2} + \frac{x_0^2 - 4x_0 - 8}{x_0^2} \ln(1+x_0), \quad (4)$$

where the parameter x_0 depends on the laser photon frequency. It should be chosen such that possible onset of e^+e^- pair production between laser photons and backscattered photons is avoided. This constraint leads to an γe energy

¹Here the source electron beam and the laser photon beam are assumed to be unpolarized.

spectrum which peaks close to its maximum at $0.83 \sqrt{s_{e^+e^-}}$. 'Realistic' cross sections are then evaluated by folding the basic SM cross section of sect. 2 with the photon spectrum (4). The results so obtained are summarized in Tab. 2, for the total, the Higgs ($M_H = 80$ GeV), the top ($m_t = 180$ GeV) and the Z/γ^* contributions at $\sqrt{s_{e^+e^-}} = 0.5, 1.0, 1.5$ and 2.0 TeV.

Table 2: Laser spectrum convoluted cross sections (in fb) of reaction (1) and different subreactions as discussed in the text at different e^+e^- cm energies.

$\sqrt{s_{e^+e^-}}$, TeV	0.5	1.0	1.5	2.0
$\sigma(\text{total})$	41.5(7)	187(2)	314(8)	420(4)
$\sigma(M_H = 80 \text{ GeV})$	15.6(1)	76.8(1)	136.3(2)	186.9(2)
$\sigma(m_t = 180 \text{ GeV})$	14.4(1)	49.0(1)	71.8(1)	86.7(2)
$\sigma(Z/\gamma^*)$	11.4(1)	62.1(4)	113(1)	159(1)

Clearly, the cross section reduction due to the convolution is largest at 0.5 TeV (about 50%) and becomes smaller with increasing energy; e.g. at 2 TeV an event loss of $\sim 30\%$ is expected. For completeness, Tabs. 3 and 4 show the Higgs and top cross sections for various M_H and m_t values as a function of $\sqrt{s_{e^+e^-}}$.

It is encouraging that even after degradation of the basic cross sections by appropriate photon flux convolution, an electron-photon collider can considerably improve the physical capabilities of Higgs and top studies. Examples are presented in the next section. It is also worthwhile to note that event rates for reactions (1)-(3) from Weizsäcker-Williams and beamstrahlung photons in an underlying e^+e^- collider are expected to be significantly below the laser induced γe collision rates [5, 7].

5 Wtb coupling and the measurement of the matrix element $|V_{tb}|$

Measurements of $|V_{tb}|$ or the partial width Γ_{tWb} , which are related in the SM, are known to be nontrivial. Recently it has been suggested to use the single top

Table 3: Laser spectrum convoluted cross sections (in fb) of reaction (3) for different e^+e^- cm energies and Higgs masses.

$\sqrt{s_{e^+e^-}}$, TeV	0.5	1.0	1.5	2.0
$\sigma(M_H = 80 \text{ GeV})$	15.6(1)	76.8(1)	136.3(2)	186.9(2)
$\sigma(M_H = 100 \text{ GeV})$	12.8(1)	70.7(1)	128.8(2)	178.7(3)
$\sigma(M_H = 120 \text{ GeV})$	10.2(1)	64.5(1)	121.0(2)	170.2(3)
$\sigma(M_H = 140 \text{ GeV})$	7.81(1)	58.4(1)	113.0(2)	161.1(3)

Table 4: Laser spectrum convoluted cross sections (in fb) of reaction (2) for different e^+e^- cm energies and top masses.

$\sqrt{s_{e^+e^-}}$, TeV	0.5	1.0	1.5	2.0
$\sigma(m_t = 160 \text{ GeV})$	17.5(1)	54.0(1)	77.1(2)	91.8(2)
$\sigma(m_t = 180 \text{ GeV})$	14.4(1)	49.0(1)	71.8(1)	86.7(2)
$\sigma(m_t = 200 \text{ GeV})$	11.8(1)	45.1(1)	67.9(1)	82.8(2)

quark reaction $e^+e^- \rightarrow \nu tb$ at high energies [7] which offers the possibility to obtain a relatively precise value of $|V_{tb}|$. In this channel, the $|V_{tb}|$ measurement capability relies mainly on the Weizsäcker-Williams photon exchange contributions, $\gamma^*e \rightarrow \nu bt$. Using however the laser backscattered high energy photon beam instead of γ^* the cross sections are typically enhanced by a factor of 3-5. As outlined in the previous sections, reaction (1) involves to a great extent νbt events involving the Wtb coupling. Their rate is directly proportional to $|V_{tb}|^2$.

The top quark is not observed directly; it decays into a W and a b quark, leading to the final state $\nu b \bar{b} W$. The extraction of the top out of this 4-body final state can however be easily achieved as seen from Fig. 5, where the invariant masses of the W and the b are shown for four energies. Clear top signals exist

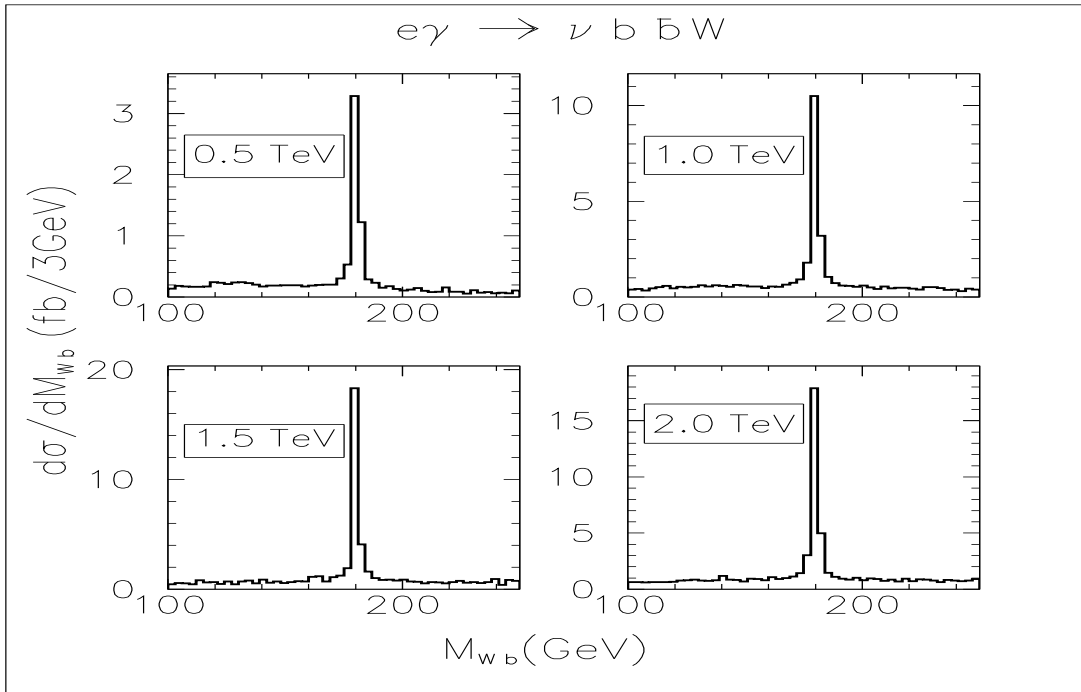


Figure 5: Differential cross sections $d\sigma/dM_{Wb}$ of reaction (1) as function of M_{Wb} .

on a small and smooth background. Selection of the top event requires only a cut around m_t and no further demands.

Using expected e^+e^- luminosities as proposed in ref. [11], an $e-\gamma$ conversion factor of 0.8 and a 30% νbt event detection probability (due to cuts to observe the top decay products and the b -jet and to eliminate backgrounds; major backgrounds are expected from the reactions $\gamma e \rightarrow \nu W Z$ and $\gamma e \rightarrow e W^+ W^-$), the two-standard deviation errors on $|V_{tb}|$ are shown in Tab. 5. As can be seen, the CKM matrix element $|V_{tb}|$ can be probed with high accuracy. Since $\delta|V_{tb}|$ is proportional to $1/\sqrt{N}$, where N is the number of events expected, the $|V_{tb}|$ measurement accuracy anticipated from reaction (2) is competitive also at lower luminosities. We would like to emphasize that the accuracy of $|V_{tb}|$ expected at

Table 5: Two-standard deviation error of $|V_{tb}|$ expected for the annual luminosities as indicated.

$\sqrt{s_{e^+e^-}}$, TeV	0.5	1.0	1.5	2.0
\mathcal{L} fb $^{-1}$	50	200	300	500
$\delta V_{tb} $	8%	2%	1.5%	1%

$\sqrt{s_{e^+e^-}} \simeq 0.5$ TeV is very similar to the expectations from the Tevatron and the LHC [12]. In particular, Willenbrock cited [13] the following one-standard deviation errors for $|V_{tb}|$: $\sim 10\%$ for Tevatron (Run II), $\sim 5\%$ for Tevatron (Run III) and $\sim 5\%$ for the LHC. However, an e^+e^- collider at energies $\sqrt{s_{e^+e^-}} \gtrsim 1.5$ TeV provides by means of the reaction $\gamma e \rightarrow \nu b t$ a somewhat better determination of $|V_{tb}|$ even for half of the luminosities anticipated in Tab. 5.

6 Probing the HWW coupling

Reaction (1), $\gamma e \rightarrow \nu b \bar{b} W$, involves also significant Higgs production (according to the diagrams (1)-(3) in Fig. 1) with a rate directly proportional to the HWW coupling. In recent years, the SM of electroweak interactions has been beautifully confirmed. In particular, Z production and its decay at LEP-1 provided Z -two-fermion couplings to be in agreement with theoretical predictions at a 1% level or better. The bosonic sector however has been much less investigated, mainly due to low energies available up to now. With the onset of next generation of e^+e^- linear colliders studies of gauge boson interactions with e.g. the Higgs boson become crucial in order to find out how the $SU(2) \otimes U(1)$ symmetry is broken. In the SM the Higgs-vector boson vertices are uniquely determined. Deviations from these couplings can occur in models with e.g. non-pointlike character of the bosons or through interactions beyond the SM at high energy scales. In the following we do not specify a particular model to search for non-SM coupling effects; rather we consider a class of models which can be parametrized by introducing an effective non-renormalizable Lagrangian which preserves the SM gauge group

$$\mathcal{L}_{eff} = \mathcal{L}_{SM} + \sum_{k=1}^{\infty} \frac{1}{(\Lambda^2)^k} \sum_i f_i^{(k)} Q_i^{d_k} \quad , \quad (5)$$

where $d_k = 2k + 4$ denotes the dimension of operators and Λ is the energy scale of new interactions. We limit ourselves to the complete set of the effective dimension-6 operators as outlined in ref. [14]. Under this restriction phenomenological applications to anomalous Higgs couplings have been discussed in [15]-[20]. In our study we adopted the notation of ref. [16] in which the effective Lagrangian contains only four operators to describe the HWW coupling. Further limitation to a custodial $SU(2)$ symmetry [21] as proposed in ref. [20], leads to only two operators relevant for the Higgs process (3), $\gamma e \rightarrow \nu W H$:

$$\frac{1}{\Lambda^2} \left\{ \frac{1}{2} f_\varphi \partial_\mu (\Phi^+ \Phi) \partial^\mu (\Phi^+ \Phi) + f_{WW} \Phi^+ (\hat{W}_{\mu\nu} \hat{W}^{\mu\nu}) \Phi \right\}. \quad (6)$$

Introducing such an effective HWW interaction in the program package CompHEP and varying the parameters F_i defined by

$$\begin{aligned} F_\varphi / (1 \text{TeV}^2) &= f_\varphi / \Lambda^2 & \text{and} \\ F_{WW} / (1 \text{TeV}^2) &= f_{WW} / \Lambda^2 \end{aligned} \quad (7)$$

within 'reasonable' ranges, the impact on the cross section of reaction (3) is investigated. Natural values of F_i are of $\mathcal{O}(1)$; when anomalous contributions to the HWW coupling vanish, i.e. $F_i \rightarrow 0$, the SM is recovered. For simplicity, the reaction (3) cross sections are now calculated in the unitary gauge instead of the t'Hooft-Feynman gauge used so far in the paper. We have also checked that they are gauge invariant within the accuracy achieved. The corresponding Feynman rules which follow from the Lagrangian (5) and (6) are presented in the Appendix.

Probing the HWW coupling involves calculating the dependence of the cross section of reaction (3) on the parameters F_i and comparison with the SM expectation. Because of the restriction to the dimension-6 operators from the beginning, the parameters F_i cannot be varied simultaneously and the cross section should only depend linearly on F_i . Otherwise, nonlinear terms in F_i or mixed terms of $F_i F_j$ with an energy scale dependence of Λ^{-4} would occur. Such terms are however excluded from our study by omitting higher than dimension-6 operators. The $\nu W H$ events are easily extracted from the 4-body final state $\nu b \bar{b} W$ of reaction (1) by imposing a cut on the $b \bar{b}$ invariant mass, $M_H - 3 \text{ GeV} < M(b \bar{b}) < M_H + 3 \text{ GeV}$, as seen in Fig. 6. Fig. 7(8) shows the Higgs cross section as function of $F_\varphi (F_{WW})$ for $F_{WW} (F_\varphi) = 0$, at $\sqrt{s_{e^+e^-}} = 0.5, 1.0, 1.5$ and 2.0 TeV for $M_H = 80 \text{ GeV}$. In both Figures, the parameter F_i ranges between -5 and $+5$ and, as can be seen, deviations from linearity occur at higher energies. In order to estimate the ranges of F_i which can be probed within our assumptions, we determined those variations of the F_i which leave the cross section unchanged within 2 s.d. from the SM value. Only statistical errors of the cross sections

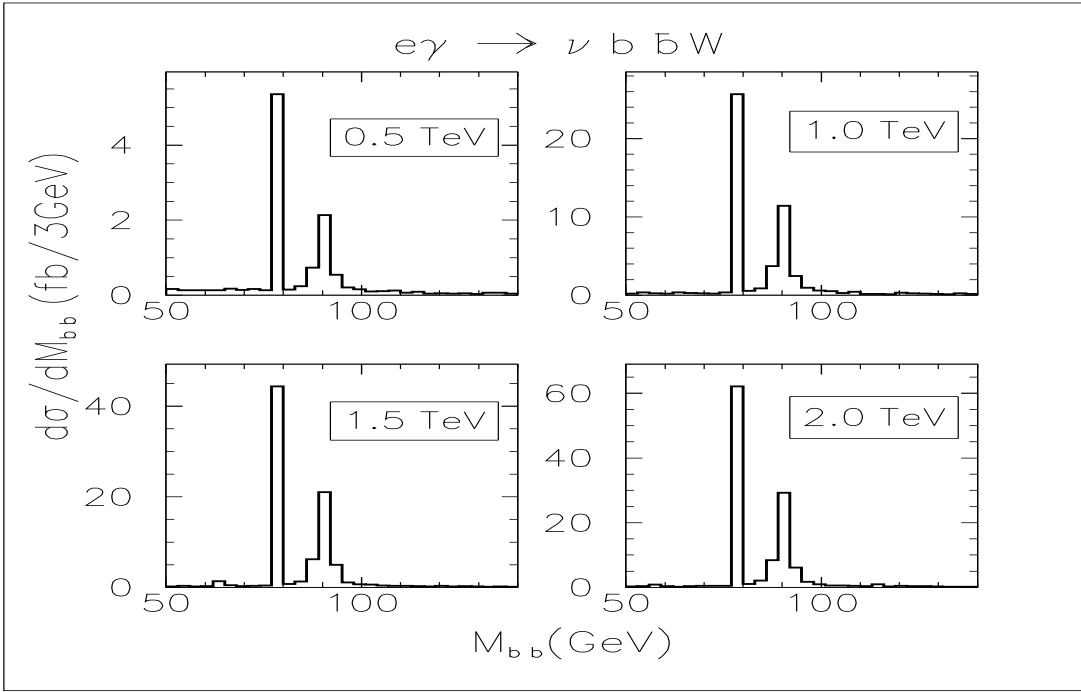


Figure 6: Differential cross sections as a function of the $b\bar{b}$ invariant mass at e^+e^- cm energies of 0.5, 1.0, 1.5 and 2.0 TeV. Clear H^0 and Z peaks are visible on a very small background.

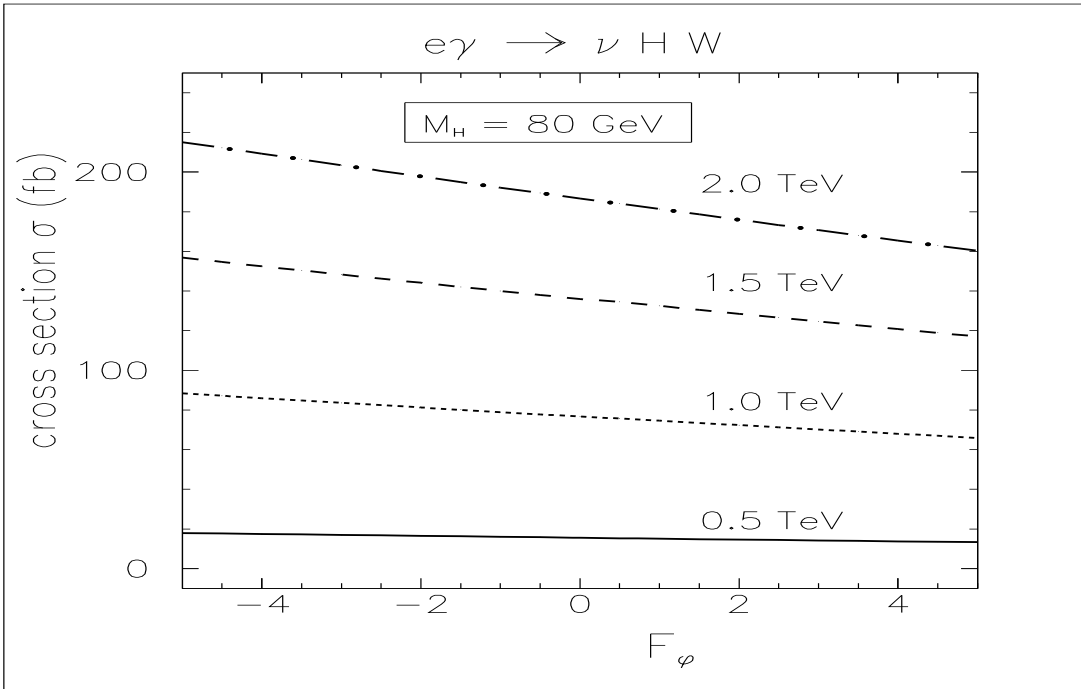


Figure 7: Cross sections for reaction (3) as function of the parameter F_ϕ with $F_{WW} = 0$, at e^+e^- cm energies of 0.5, 1.0, 1.5 and 2.0 TeV for $M_H = 80$ GeV.

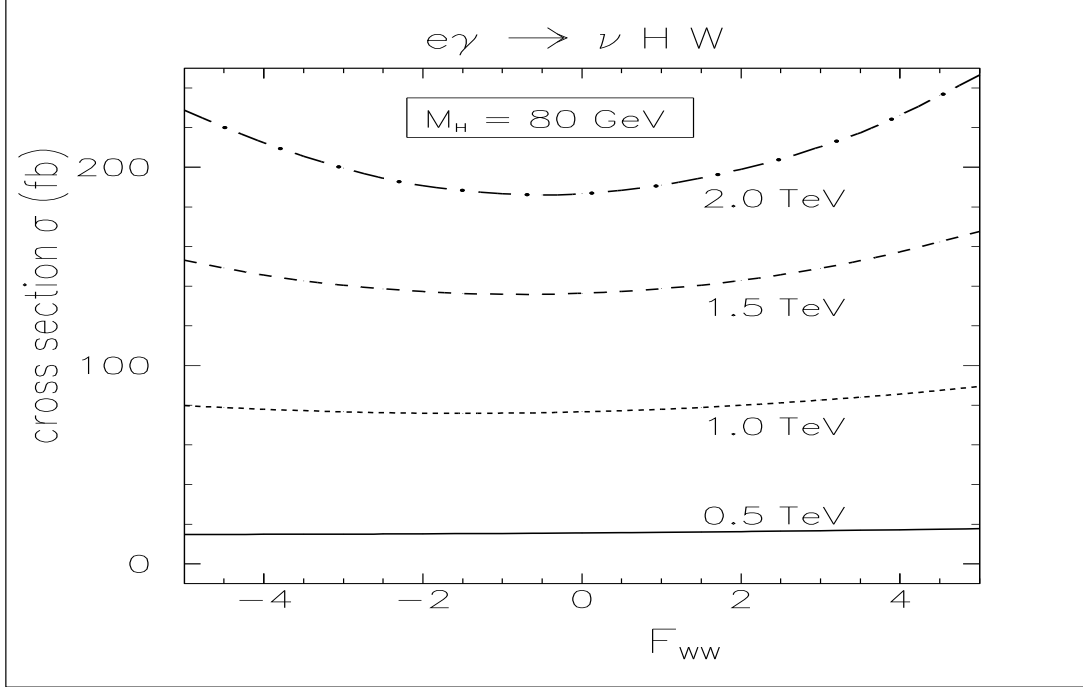


Figure 8: Cross sections for reaction (3) as functions of the parameter F_{WW} with $F_\varphi = 0$, at e^+e^- cm energies of 0.5, 1.0, 1.5 and 2.0 TeV for $M_H = 80$ GeV.

were considered taking into account the integrated luminosities of Tab. 5, an $e-\gamma$ conversion factor of 0.8 and a 30% νHW detection probability. In addition, it has been checked that the cross sections in the F_i intervals so obtained are in accord with a linear behaviour as required by the restriction on dimension-6 operators. The intervals of F_i obtained are presented in Tab. 6.

Table 6: Range of $|F_\varphi|$ and $|F_{WW}|$ obtained from the two-standard deviation criteria as described in the text.

$\sqrt{s_{e^+e^-}}$, TeV	0.5	1.0	1.5	2.0
$ F_\varphi $	5.0	1.0	0.6	0.4
$ F_{WW} $	9.0	2.5	2.0	1.0

Clearly, only at energies $\gtrsim 1$ TeV the total cross section of $\gamma e \rightarrow \nu WH$ involves some sensitivities to the anomalous couplings considered. Recent analyses of e.g. the simpler two-body reactions $e^+e^- \rightarrow H\gamma$ or HZ [19, 20] revealed high sensitivities for these operators including production and decay angular distri-

butions. We expect that by inclusion of differential distributions or the whole phase space event population the sensitivity with respect to the $|F_i|$ becomes larger. Such a study including additional 3-body final states is in preparation and will be published in a forthcoming paper. At present, we would like to point out that the process $\gamma e \rightarrow \nu WH$ is of interest at $\sqrt{s_{e^+e^-}} = 1\text{-}2$ TeV since it becomes sensitive and comparable to other reactions to probe the structure of operators. In this respect the disentangling of the origin of 'new physics' may be further helped by comparing analyses of different reactions.

7 Summary

Results of a complete tree-level calculation for the reaction $\gamma e \rightarrow \nu b \bar{b} W$ at cm energies 0.5 to 2.0 TeV are presented and discussed, using the computer package CompHEP. This reaction is very interesting on its own because it involves at the same time single top production, $\gamma e \rightarrow \nu \bar{b} t$, and associated Higgs production, $\gamma e \rightarrow \nu HW$, with subsequent decays of $t \rightarrow Wb$ and $H \rightarrow b \bar{b}$, respectively. Therefore, both three-body reactions already studied in previous publications are analyzed in an extended manner taking into account interferences between different subchannels and the irreducible background.

We present the total cross sections of reaction (1) as well as those of its main components as functions of $\sqrt{s_{\gamma e}}$ and $\sqrt{s_{e^+e^-}}$, the latter after convolution with the backscattered photon flux of ref. [1]. Above threshold, Higgs and Z/γ^* (with $H \rightarrow b \bar{b}$ and $Z/\gamma^* \rightarrow b \bar{b}$ decays) contribute with about equal weights to the total rate while single top production is roughly a factor 2 lower. The Higgs and the top production cross sections are only weakly dependent on the Higgs mass in the range 80 to 140 GeV and the top mass between 160 and 200 GeV. The contributions from multiperipheral diagrams are very small. They grow however with increasing energy. Interferences between different subchannels were found to be significant only at the highest energies. They are to some extent compensated by the multiperipheral contributions.

The event rate for the reaction $\gamma e \rightarrow \nu tb$, which is large even after folding with an energy spectrum of the backscattered photon beam and making reasonable assumptions on collider luminosities and detection probabilities, provides a very sensitive measurement for the CKM matrix element $|V_{tb}|$. If the cross section for single top production is measured with high accuracy, the two-standard deviation errors on $|V_{tb}|$ can be close to (1-3)% at $\sqrt{s_{e^+e^-}} = 1\text{-}2$ TeV. To our knowledge such an accuracy cannot be achieved by other measurements so far considered.

The reaction $\gamma e \rightarrow \nu HW$ allows to probe the HWW coupling and to

measure parameters of dimension-6 operators in the effective Lagrangian. It has been found that at 0.5 TeV the accuracy obtained on these parameters is not sufficient to make this measurement sensitive to new physics while at energies $\sqrt{s_{e^+e^-}} = 1\text{-}2$ TeV the HWW coupling can be probed with high sensitivity and deviations from the Standard Model could show up.

Appendix

The Feynman rules for HWW and $HWW\gamma$ vertices in unitary gauge which follow from the effective Lagrangian (5) and (6):

$$\begin{aligned} \Gamma_{\mu\nu}^{HWW}(p, q, \kappa) = & \frac{eM_W}{s_W} \left\{ \left(1 - \frac{1}{4}f_\varphi \frac{v^2}{\Lambda^2}\right) g_{\mu\nu} \quad + \right. \\ & \left. + 2f_{WW} \frac{1}{\Lambda^2} [g_{\mu\nu}(q, \kappa) - q_\nu \kappa_\mu] \right\} \end{aligned} \quad (8)$$

and

$$\begin{aligned} \Gamma_{\mu\nu\alpha}^{HWW}(p, q, \kappa, l) = & \frac{e^2 M_W}{s_W} 2f_{WW} \frac{1}{\Lambda^2} \left\{ g_{\mu\nu}(q - \kappa)_\alpha \quad - \right. \\ & \left. - q_\nu g_{\mu\alpha} + \kappa_\mu g_{\nu\alpha} \right\} \end{aligned} \quad (9)$$

where $v = \frac{2M_W}{e}s_W$ is the vacuum expectation value; p, q, κ and l are the momenta of the H, W^+, W^- and γ fields, respectively. The Lorentz indices of the W 's and γ fields are denoted as μ, ν and α , respectively. The quantity 1 in the first term of $\Gamma_{\mu\nu}^{HWW}$ corresponds to the SM vertex. The second vertex $\Gamma_{\mu\nu\alpha}^{HWW}$ does not occur in the SM at tree level.

Acknowledgements

E.B. and A.P. are grateful to DESY IfH Zeuthen for the kind hospitality, and to P. Söding for his interest and support. The work has been supported in part by the RFBR grants 96-02-19773a and 96-02-18635a, and by the grant 95-0-6.4-38 of the Center for Natural Sciences of State Committee for Higher Education in Russia.

References

- [1] I.F. Ginzburg, G.L. Kotkin, V.G. Serbo and V.I. Telnov, Pisma ZhETF 38 (1981) 514; Nucl. Instr. and Meth. **205** (1983) 47; V.I. Telnov, Nucl. Instr. and Meth. **A294** (1990) 72.

- [2] R.H. Milburn, Phys. Rev. Lett. **10** (1963) 75;
F.R. Arutyunyan and V.A. Tumanyan, Sov. Phys. JETP 17 (1963)1412.
- [3] S. L. Glashow, Nucl. Phys. **22** (1961) 579;
S. Weinberg, Phys. Rev. Lett. **19** (1967) 1264;
A. Salam, Elementary Particle Theory, ed. by N. Svartholm, Stockholm (1968) 367.
- [4] C.F. Weizsäcker, Z. Phys. **88** (1934) 612;
E.J. Williams, Phys. Rev. **45** (1934) 729.
- [5] E. Boos, M. Dubinin, V. Ilyin, G. Jikia, A. Pukhov and S. Sultanov, Phys. Lett. **B273** (1991) 173;
K. Hagiwara, I. Watanabe and P.M. Zerwas, Phys. Lett. **B278** (1992) 187;
K. Cheung, Phys. Rev. **D48** (1993) 1035.
- [6] G. Jikia, Nucl. Phys. **B374** (1992) 83;
E. Yehudai, S. Godfrey and K.A. Peterson, Proc. of the Workshop on Physics and Experiments with Linear e^+e^- Colliders, Waikoloa, Hawaii, April 26-30, 1993, p.569.
- [7] E. Boos, Y. Kurihara, Y. Shimizu M. Sachwitz, H.J. Schreiber and S. Shichanin, Z. Phys. **C70** (1996) 255.
- [8] E. Boos, M. Dubinin, V. Ilyin, A. Pukhov and V. Savrin, Moscow State University preprint SNUTP-94-116, Oct 1994 and Korean Physical Society meeting, October 21, 1994 (hep-ph/9503280).
- [9] Particle Data Group, Phys. Rev. **D50** (1994) 1.
- [10] V.A. Ilyin, D.N. Kovalenko and A.E. Pukhov, INP MSU Preprint-95-2/366, Moscow State University, (1995).
- [11] B.H. Wiik, talk given at the TESLA meeting, Frascati, Nov. 1994.
- [12] A.P. Heinson, A.S. Belyaev and E.E. Boos, Proc. of the Workshop on Physics of the Top Quark, Iowa State University, Ames, Iowa (1995);
T. Stelzer and S. Willenbrock, Phys. Lett. **B357** (1995) 125.
- [13] S. Willenbrock, talk given at the 28th International Conference on High Energy Physics, 25-31 July 1996, Warsaw, Poland.
- [14] W. Buchmüller and D.Wyler, Nucl. Phys. **B268** (1986) 621.
- [15] K. Hagiwara, S. Ishihara, R. Szalarski and D. Zeppenfeld, Phys. Rev. **D48** (1993) 2182.

- [16] K. Hagiwara, R. Szalarski and D. Zeppenfeld, Phys. Lett. **B318** (1993) 155.
- [17] K. Hagiwara and M.L. Stong, Z. Phys. **C62** (1994) 99.
- [18] B. Grzadkowski and J. Wudka, Phys. Lett. **B364** (1995) 49.
- [19] G.J. Gounaris, F.M. Renard and N.D. Vlachos, Nucl. Phys. **B459** (1996) 51;
G.J. Gounaris, J.Layssac, J.E. Paschalis, F.M. Renard and N.D. Vlachos, preprint PM/96-08 and THEP-TP 96/02.
- [20] W. Kilian, M. Krämer and P.M. Zerwas, preprint DESY 95-217, 1995.
- [21] P. Sikivie, L. Susskind, M. Voloshin and V. Zakharov, Nucl. Phys. **B173** (1980) 189;
G.J. Gounaris and F.M. Renard, Z. Phys. **C59** (1993) 143.